

Status of studies on high-temperature oxidation and quench behaviour of Zircaloy-4 and E110 cladding alloys

M. Steinbrück¹, J. Birchley², A.V. Goryachev³, M. Grosse¹, T. J. Haste², Z. Hozer⁴,
A.E. Kisselev⁵, V.I. Nalivaev⁶, V.P. Semishkin⁷, L. Sepold¹, J. Stuckert¹, N. VÉR⁴, M.S. Veshchunov⁵

CONTRACT SARNET FI60-CT-2004-509065

1) FZK, Karlsruhe (DE)
2) PSI, Villigen (CH)
3) RIAR, Dimitrovgrad (RU)
4) AEKI, Budapest (HU)

5) IBRAE, Moskau (RU)
6) LUCH, Podolsk (RU)
7) GIDROPRESS, Podolsk (RU)

SUMMARY

This paper gives an overview on the status of knowledge of high-temperature oxidation of the two zirconium alloys Zircaloy-4 and E110 with special emphasis on results obtained during the SARNET period. The tin-bearing alloy Zircaloy-4 and the niobium-bearing alloy E110 are the materials for cladding and structures recently mainly used in pressurised water reactors of the Western type and VVERs and RBMKs, respectively.

Results of separate-effects tests, single-rod tests, and large-scale bundle experiments are summarised. Focus is directed to oxidation kinetics at high temperature, hydrogen release and absorption by the remaining metal, and behaviour during quenching.

Both materials behave very similarly as long as the superficial oxide scales formed during oxidation are dense and protective. Main differences are seen in connection with breakaway oxidation which leads to enhanced oxidation and hydrogen uptake and thus embrittlement and early failure of the cladding. The temperature range at which pronounced breakaway is observed is different for the two alloys.

The status of modelling of oxidation kinetics, thermo-mechanical behaviour during cool-down and the influence of irradiation are discussed at the end of the paper.

A Introduction

Zirconium alloys are widely used in nuclear and chemical industries because of their low neutron absorption and their excellent mechanical and corrosion properties. The classical zirconium alloy for nuclear applications in western pressurised water reactors (PWR) is Zircaloy-4 with approx. 1.5 wt% tin as major alloying element. It is used for fuel cladding, control rod guide tubes, and grid spacers. A huge data base is available for this alloy regarding the oxidation kinetics over a wide range of temperatures from operational conditions (~600 K) to temperatures expected for hypothetical severe accidents (>2000 K) [1, 2]. Currently Zircaloy-4 is being substituted by advanced cladding materials optimised for high burnup and long operation times in nuclear power plants (NPP). Nevertheless, the oxidation correlations of computer codes simulating accident scenarios today mainly rely on Zircaloy-4 data. It is noted that almost all the computer codes in current use assume a parabolic kinetic law, i.e. mass gain is proportional to the square root of time.

In Russia the niobium-bearing alloy E110 (Zr1%Nb) is used for cladding and structure materials in RBMK and VVER nuclear reactors for many years. This material has been extensively investigated, too, mainly in Russian and Eastern European laboratories; but the publicly available data are scarce [3, 4, 5, 6].

Comparative studies show superior resistance to oxidation of either E110 or Zry-4 depending on test conditions, especially on temperature and atmosphere. Recently, numerous separate-effects tests on high-temperature oxidation of various cladding alloys, including E110 and Zry-4, in different atmospheres have been conducted [7, 8, 9] in Germany and Hungary.

Further tests including quenching have been conducted in single-rod test rigs in Russia (in the frame of the ISTC Project #1648.2) and Germany. The Russian tests at RIAR Dimitrovgrad additionally included experiments with irradiated fuel rod segments. Although fission product release is beyond the scope of this paper, noticeable differences between fresh and irradiated cladding behaviour connected with strong embrittlement and fragmentation of irradiated fuel rods and their mechanistic interpretation will be briefly discussed in this paper.

Furthermore, bundle tests including high-temperature oxidation and quenching with E110 were conducted in the PARAMETER facility at LUCH (Russia, ISTC project), in the CODEX facility in Hungary, and with both materials in the QUENCH facility at FZK, Germany. Two tests, namely QUENCH-06 (with Zry-4) and QUENCH-12 (with E110) were conducted with similar test protocols, but showed quite different results regarding oxidation and hydrogen source term.

This paper summarises the "historical" and the most recent (obtained within SARNET) results on high temperature oxidation, hydrogen source term and hydrogen absorption of both zirconium alloys including the behaviour during quenching from high temperatures. The consideration of different properties in computer codes for simulation of nuclear accidents will be discussed as well as the need for further development taking into account the differences of the cladding materials.

Finally, an outlook will be given on future experiments planned to be performed within SARNET-2 and ISTC with special emphasis on future QUENCH and PARAMETER bundle tests and planned separate-effects tests on advanced cladding alloys.

B Experimental results

B.1 Separate-effects tests

B.1.1 Overview on earlier experiments with Zry-4 and E110

The first high temperature experiments with Zr-cladded fuel in steam atmosphere conducted in the USA in the 1960s indicated that the cladding can lose its integrity well below the melting temperature of Zircaloy-4. The failure happened during the tests or during post-test handling of the specimens due to the embrittlement of zirconium after oxidation in steam. Loss of cladding ductility was observed in both small-scale laboratory tests and in-pile experiments TREAT and SPERT [10]. Metallographic examinations pointed out that the embrittlement was caused by microstructural changes in the cladding. The cross section of brittle cladding contained oxide layer, oxygen stabilised α -phase layer and the region of prior β -phase. It was understood that the high temperature oxidation of Zircaloy can result in the

embrittlement of cladding, and the brittle material can fragment during the quenching phase of a reactor accident.

In the 1970s and 1980s several experimental series with Zircaloy oxidation were carried out in the USA, Japan, Germany and France [10, 11]. Most of the tests supported the understanding of fuel behaviour under design basis accidents and focused on the development of safety criteria for LOCA events [44]. Oxidation kinetics were investigated in details in those tests, and several correlations were produced for Zircaloy-4 cladding in different laboratories [11]. The correlations were implemented into fuel behaviour and severe accident simulation codes that are widely used today for the prediction of the consequences of reactor accidents.

Later on the investigation of high-temperature behaviour of E110 cladding started, as reviewed in the EU 3rd Framework Programme [45]. The first results on E110 cladding oxidation and deformation at high temperatures were reported by Solyany in the early 1980s [13]. The experimental series launched by Vrtilkova in 1984 [12] showed noticeable differences between Zircaloy-4 and E110 at temperatures between 700 and 1050 °C. The typical oxide layer of E110 was found characteristic for spalling (breakaway oxidation) at temperatures 700-1000 °C while the Zircaloy-4 showed breakaway pronounced at the most between 950 and 1050 °C. Both alloys revealed mainly compact oxide scales outside the indicated temperature regions.

Several other comparative tests were carried out in Germany [3], Russia [5] and Hungary [9] with Zircaloy-4 and E110 claddings. The experimental results pointed out that both claddings can fail during quenching at different degrees of oxidation. Due to the observed differences in cladding behaviour, new correlations and models had to be introduced into the corresponding codes. Today it is well understood that the fast embrittlement of claddings is mainly caused by breakaway oxidation, which makes way to the uptake of hydrogen by the Zr through cracks in the oxide scale. More compact oxide scales prevent intense hydrogen uptake and keep the cladding ductile till a higher degree of oxidation.

The current experimental series with E110 and Zircaloy-4 claddings cover the effects of different atmospheres, cladding pre-oxidation to simulate normal operation and the role of temperature histories. An important part of the investigations is devoted to high burnup effects in the cladding and to the introduction of new cladding types and fabrication technologies. The current experimental data make possible the significant extension of available databases (see e.g. [14]) and further development of numerical models.

B.1.2 Isothermal tests in steam

Isothermal steam oxidation tests were performed recently within SARNET in flowing argon/steam atmosphere using a resistance-heated vertical tube furnace [7]. The temperatures varied between 800 and 1400 °C.

The expected parabolic time dependence given in Eq. (1) was found for both materials at all temperatures investigated, at least at the beginning of the oxidation (see Fig. 1).

$$\Delta m = \delta_m \cdot \sqrt{t} \quad (1)$$

Δm is the mass increase, δ_m the mass increase rate and t the time. In Fig. 2 the temperature dependences of mass increase rates are given for both materials. These temperature

dependences can be described by two Arrhenius functions given in Eq. (2) corresponding to the different oxide crystal structures.

$$\delta_m = \delta_m^* \cdot e^{\frac{Q}{RT}} \quad (2)$$

Q is the activation energy; the values determined are given in Tab. 1; R is the universal gas constant. The transformation in the activation energy is about 50 K lower for E110 than for Zry-4. In the higher temperature range the activation energy of Zry-4 is lower than that of E110. In the lower temperature range it is opposite. However, the starting point for oxide breakaway at E110 can influence this finding.

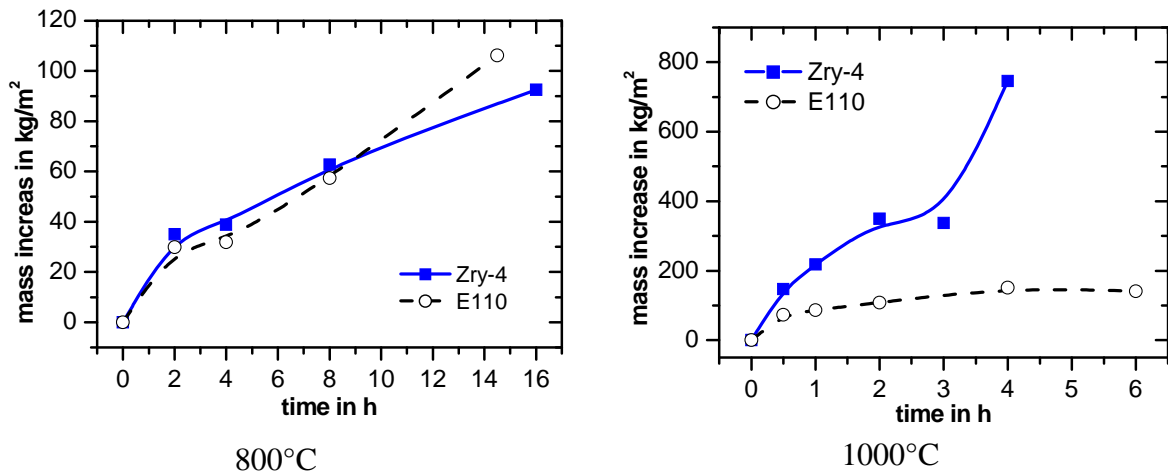


Fig. 1: Oxidation kinetics of E110 and Zry-4 at 800 and 1000°C

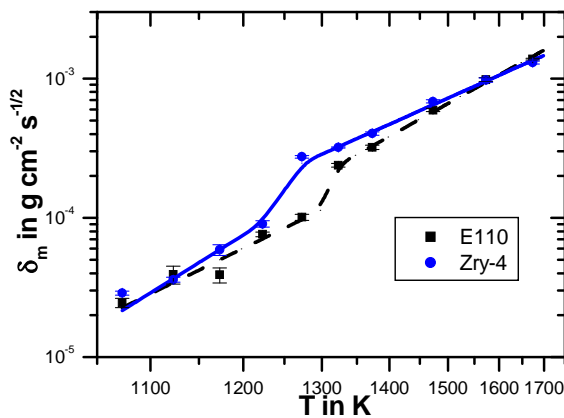


Fig. 2: Comparison of the temperature dependences of mass increase rate of E110 and Zry-4

The breakaway effect was observed at about 1000 °C for Zry-4 and in the range of 800 to 1000 °C for E110. At these temperatures the oxidation starts also with parabolic time dependence. From there going up in temperature a linear function is found. The morphology of the spalled oxide is different between the two materials. These oxide layers are much finer for E110 than for Zry-4. At a first sight the comparison suggests a much lower oxidation rate of E110. However, during the experiments a lot of the spalled oxide of E110 got lost in the furnace. Therefore, the mass increase of this material was determined as too low in the temperature range where breakaway occurs.

Table 1: Activation energies (Q in Eq. 2) of steam oxidation for E110 and Zry-4.

E110		Zry-4	
$1073 \text{ K} \leq T < 1273 \text{ K}$	82690 J/(mol K)	$1073 \text{ K} \leq T \leq 1223 \text{ K}$	105210 J/(mol K)
$1323 \text{ K} \leq T \leq 1673 \text{ K}$	94210 J/(mol K)	$1273 \text{ K} \leq T \leq 1673 \text{ K}$	75100 J/(mol K)

B.1.3 TG experiments in oxygen

Thermo-gravimetric investigations have been conducted isothermally in oxygen-argon mixtures between 600 and 1100 °C as well as in transient tests up to 1580 °C [8]. These experiments confirmed the complex oxidation behaviour resulting in strong differences in oxidation rates at temperatures below 1100 °C where the already discussed breakaway oxidation plays a role. Generally, a transition from parabolic or (sub-)cubic oxidation kinetics to linear (or even faster) is observed for both alloys between 600 and 1000 °C. This transition is more abrupt for Zry-4 and more gradual for E110 at most temperatures. The critical oxide scale thickness at which breakaway starts, increases with temperature from a few microns at 600 °C to 70 and 30 µm for Zry-4 and E110, respectively, at 1000 °C. At 1100 °C and above the well known parabolic oxidation kinetics has been confirmed.

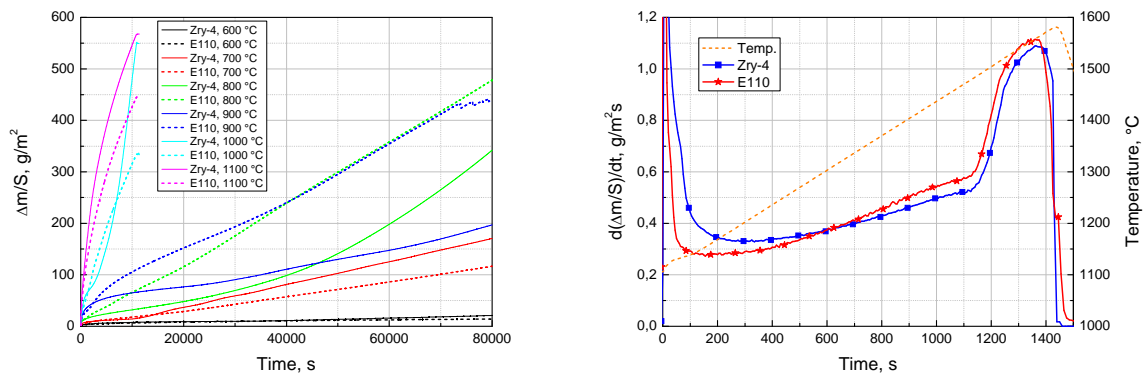


Fig. 3: Mass gain of Zry-4 and E110 cladding segments during isothermal oxidation in O_2 at 600 to 1100 °C (left); and reaction rate during transient tests from 1100 to 1600 °C (right)

Obviously, the different compositions and manufacturing procedures result in varying susceptibility for breakaway oxidation in dependence on temperature. So, E110 shows slower oxidation rates than Zry-4 at 600 and 700 °C and considerably higher rates at 800 and 900 °C. At 1000 °C the situation changes twice with time, finally resulting in severe breakaway oxidation of Zry-4. Beyond breakaway regime temperatures the kinetics are quite similar at 1300-1400 °C with a change from lower oxidation rates for the Nb alloy to the Sn alloy, as can be seen in Fig. 3.

In transient tests starting from room temperature, only E110 showed breakaway passing the relevant temperature range which is another indication of the higher susceptibility to breakaway of the Nb alloy. Discontinuous increases in oxidation rates were observed for both materials at about 1000 and 1500 °C, indicating the transition of the oxidic phases from monoclinic to tetragonal to cubic ZrO_2 with increasing sub-stoichiometry and oxygen diffusion coefficients.

B.1.4 First tests in air

The air ingress topic, especially the oxidation of Zry-4 in nitrogen-containing atmospheres has been extensively discussed in [15] and is addressed in two other papers of this conference [16, 17]. Only a few test data are available on the oxidation of E110 in air [18]. The general behaviour of both alloys regarding oxidation mechanism, kinetics, and influence of pre-oxidation on subsequent reactions in atmospheres containing air is similar.

The detrimental effect of increasing oxidation rates in air is connected with the formation of zirconium nitride under local or global oxygen starvation conditions and its re-conversion into oxide with quite different densities. Consequently, main differences are connected with the different breakaway of both alloys, allowing access of nitrogen to the metal-oxide interface.

Comparative tests at 800, 1000, and 1200 °C with Zry-4 and E110 in air-containing atmospheres have been conducted at FZK in the frame of the SARNET mobility programme [18].

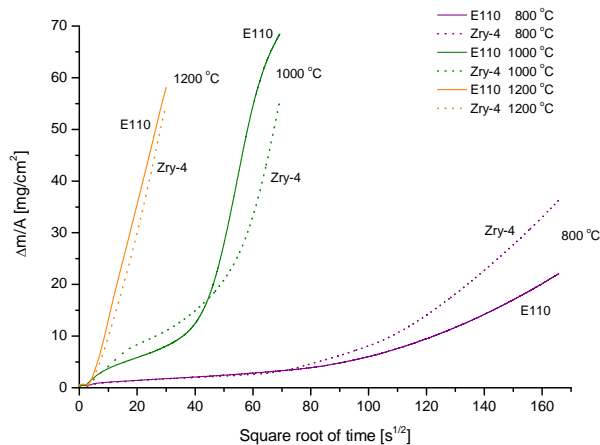


Fig. 4: Weight gain of E110 and Zircaloy-4 cladding materials during isothermal oxidation in air at 800, 1000 and 1200 °C

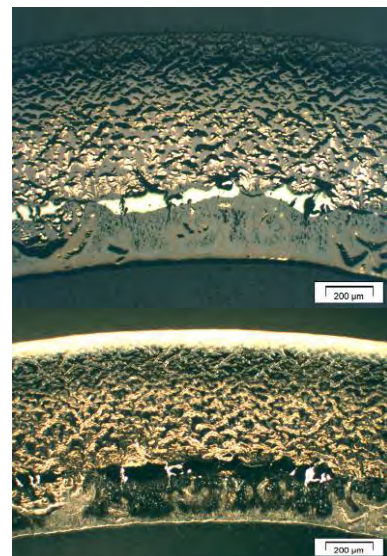


Fig. 5: Metallographic images of an E110 specimen oxidised in air at 1200 °C for 15 min (at bright and dark field)

For oxidation in air at 800 °C the transition from the parabolic to a faster kinetic is earlier (~3000 s) and more pronounced in case of Zircaloy-4 than in case of E110 (~5000 s) (see Fig. 4.).

At all investigated temperatures the reaction rate in air is higher than that in oxygen but at 1000 and 1200 °C only after a certain initial time (due to the higher temperature escalation in oxygen than in air because of lack of oxygen starvation conditions). At 1000 °C at begin of air oxidation, Zircaloy-4 shows a higher reaction rate, but from about 1200 s on E110 shows a faster reaction kinetics (till ~3800 s). At 1200 °C both E110 and Zircaloy-4 show reaction kinetics little faster than parabolic and quite similar to each other (see Fig. 4).

Metallographic cross sections look fairly similar for both alloys at all investigated temperatures. The features of oxide scales of the two cladding materials are the same, with

circumferential cracks and break into large sections after air oxidation at 800 °C. The oxide scales formed at 1000 and 1200 °C consist of oxide-nitride mixture, mainly at the phase boundary of metal and oxide. A porous oxide scale formed by re-oxidation of nitride in the outer regions (see Fig. 5).

B.2 Single rod tests

B.2.1 Quench experiments at FZK

The program on investigation of Zircaloy-4 cladding oxidation phenomena during reflood was performed at Forschungszentrum Karlsruhe during 1996-1998. A total of 22 water quench and 45 steam rapid-cooldown single rod tests with pre-oxidised claddings were performed [19-21]. The main parameters of the tests were the degree of pre-oxidation and the temperature at the onset of cooldown. Pre-oxidation of the tube specimens with a total length of 150 mm to a target oxide thickness of 100-300 µm took place at 1400 °C in a steam/argon gas mixture in the QUENCH-SR rig. Then the specimens were quenched with water or rapidly cooled down by steam which was injected into the test section. Steam cooling simulated the conditions above the quench-water front during core reflood. Four temperature levels were chosen at onset of reflood: 1100, 1200, 1400, and 1600 °C.

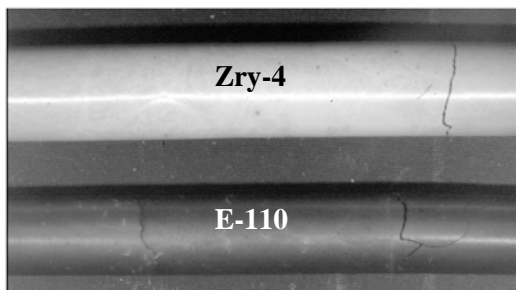


Fig. 6: Cooldown by steam from 1400 °C after preoxidation at 1400 °C with a ZrO₂ thickness of ~270 µm; post-test appearance

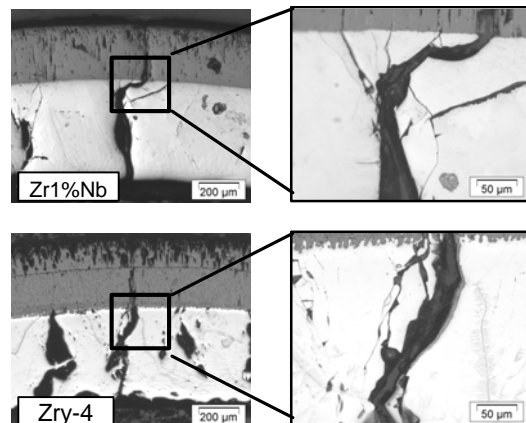


Fig. 7: Oxidation and crack formation at 1400 °C

Under similar conditions nine single rod tests with VVER fuel rod simulators (E110) have been performed with rapid cooldown by steam in the temperature range 1100 °C-1600 °C [22]. The post-test appearance of the oxidised Zr1%Nb tubes differs from that of Zircaloy-4 (Fig. 6). Particularly, the Zr1%Nb oxide surface is considerably darker. The emissivity of oxidised Zr1%Nb tube surface was measured as 0.8 whereas the emissivity of oxidised Zircaloy-4 tube surface was determined to be 0.55.

The mechanical behaviour of the cladding tubes depends on the cooldown temperature and the extent of pre-oxidation. Up to 1400 °C the kinetics of the oxide layer growth on the Zr1%Nb surface is comparable with the kinetics of ZrO₂ layer growth on the Zircaloy-4 surface. Above 1400°C the oxidation rate is higher for Zr1%Nb. The micro-cracks in the oxide layer on the Zr1%Nb tube distribute uniformly, whereas for Zircaloy-4 the micro-cracks are preferably in the outer sub-layer of the oxide scale. The formation of a through-

wall crack network with a crack density of ~ 50 mm/cm² was observed for both alloys in the steam rapid cooldown tests with a ZrO₂ layer thickness larger than 200 μ m. The thinner oxide layer induced only single longitudinal cracks. In contrast to the Zircaloy-4 tests, the oxidation of the crack surfaces was negligible for E110 (Fig. 7).

The hydrogen release during pre-oxidation and quenching phases was analysed for E110. Up to 1400°C no deviation of the hydrogen release rate from the analogous tests with Zircaloy-4 cladding was found. The amount of hydrogen generated due to crack oxidation was estimated to be less than 10% of the total hydrogen mass generated during cooldown of the Zircaloy-4 samples. Additionally, the amount of absorbed hydrogen in segments of Zr1%Nb test specimens was measured after the tests by hot extraction at 1500°C. The results show that under the same conditions the Zr1%Nb cladding tubes absorb less hydrogen (0.3-1 at % ref. to metal) than the Zircaloy-4 ones (1-3.5 at% ref. to metal).

B.2.2 Experiments with fresh and irradiated fuel rod segments at RIAR

Separate-effects tests with irradiated VVER fuel rod simulators at simulated reflood conditions have been conducted within the framework of the 1648.2 ISTC Project. Tests were aimed at the definition of hydrogen quantity produced during the quench phase with the cladding outer surface oxide layer thickness as parameter. The fuel rod simulators were made of spent commercial VVER fuel rods irradiated up to a burnup of 60 MW d/kg U. The test sequence shown in Fig. 8 includes pre-oxidation in steam at 1400 °C, heating up to a target test temperature (1400, 1600, 1700 °C) and quenching by immersing the simulator in water at a rate of 15 mm/s. On-line measurements of hydrogen production were taken during pre-oxidation and quenching.

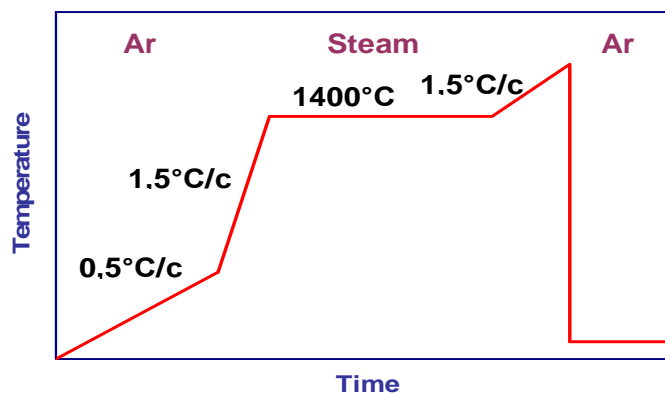


Fig. 8: Test regime

All tests have been carried out in the one-side oxidation mode. The inner cladding surface has been protected from steam oxidation by an argon flow through the simulator.

Tests with non-irradiated fuel rod simulators have shown the gradual drop of the quantity of hydrogen produced at the quench stage with the increase in oxide shell thickness (Fig. 9). Collapse of the simulators was observed only at a quench temperature of 1700 °C. It did, however, not contribute to the hydrogen production as the crack surfaces have been found not oxidized.

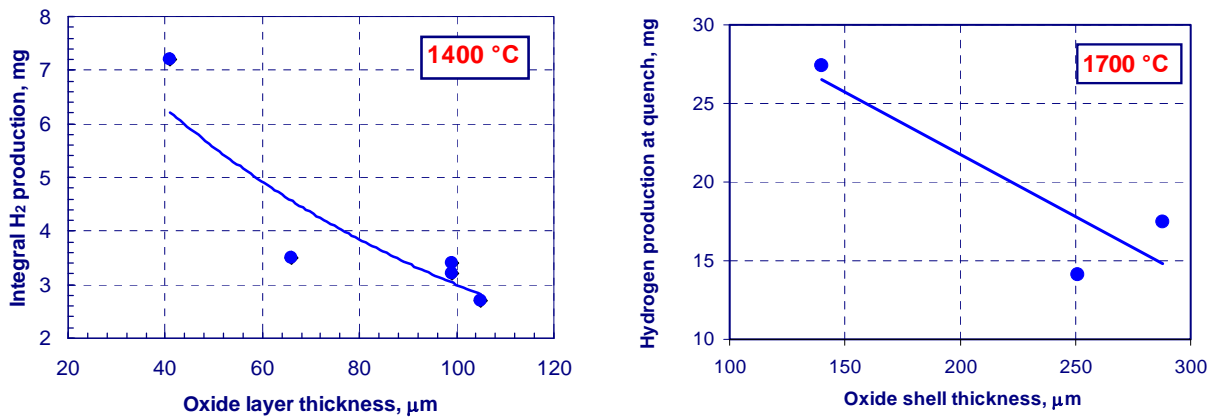


Fig. 9: Hydrogen production during quench of non-irradiated fuel rod simulators vs. oxide layer thickness

Fragmentation of the irradiated simulators was observed either at oxide layer thickness more than 100 μm or at any oxide film thickness at test temperature beyond 1600 °C.

Post-test metallographic examinations of the irradiated simulators tested without pre-oxidation have shown that the tight fuel-cladding bonding resulted in formation of the thick α -Zr(O) layer on the inner cladding surface increasing with increase of the test temperature (Fig. 10). The cladding embrittlement due to this effect resulted in fragmentation of the simulators even without pre-oxidation at temperature of 1700 °C.

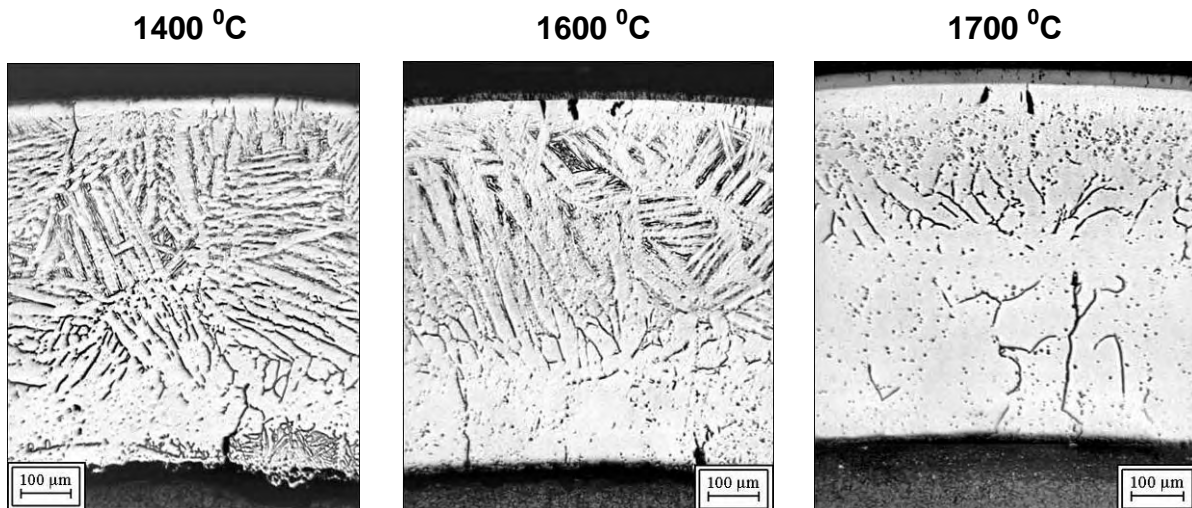


Fig. 10: Cladding structure of the non-irradiated simulators tested without pre-oxidation

In the tests with irradiated fuel rod simulators including pre-oxidation, the hydrogen production kinetics has shown that the cladding crack formation has begun during pre-oxidation increasing the hydrogen production after 8000 s oxidation that corresponds to an oxide layer thickness of about 150 μm (Fig. 11).

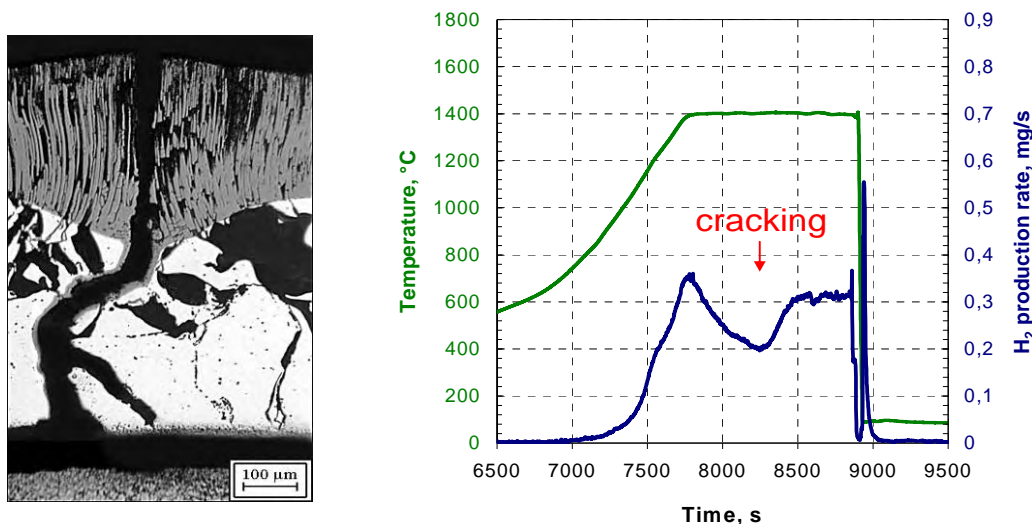


Fig. 11: Hydrogen production rate and crack formation during pre-oxidation of irradiated samples

Cladding inner surface oxidation due to fuel-cladding bonding and absence of the fuel-cladding gap are the main reasons for the different behaviour of the irradiated and fresh rods: irradiated simulators resulted in earlier fragmentation and increase of hydrogen production during the quench.

B.3 Bundle tests

B.3.1 QUENCH-12 vs. QUENCH-06

The QUENCH-12 experiment [23, 24] was carried out within the ISTC Project #1648.2 to investigate the effects of VVER materials (niobium-bearing alloys) and bundle geometry on core reflood, in comparison with test QUENCH-06 using a western-type PWR simulator bundle (Zircaloy-4) [25]. QUENCH-12 was conducted with largely the same protocol as QUENCH-06 (Fig. 12), such that the effects of VVER characteristics could be observed more easily. The scenario of the test was more typical for spent pool fuel than for reactor accidents.

While the PWR bundle uses 20 heated rods, 1 unheated central rod and 4 corner rods arranged on a square lattice, with a heated length of 1024 mm, the VVER bundle uses 13 unheated rods, 18 heated rods and 6 corner rods, arranged in a hexagonal lattice. The coolant channel area ratio between two bundles is $Q12/Q06 = 1.09$, therefore the fluid flow rates were preset 9% higher for the QUENCH-12 bundle than for the QUENCH-06 bundle to provide the same flow velocity. The bundle material mass ratio is $Q12/Q06 \sim 0.97$, the metallic surface ratio is $Q12/Q06 = 1.22$.

The steam-argon mixture, which entered the test section at the bottom, is heated with help of the bundle electric power and its preset axial power profile. The axial temperature distribution during the pre-oxidation phase shows that the greater part of the QUENCH-12 bundle was oxidised for a long period at temperatures between 1000 K and 1300 K, i.e. under conditions typical for the E110 breakaway oxidation (Fig. 13).

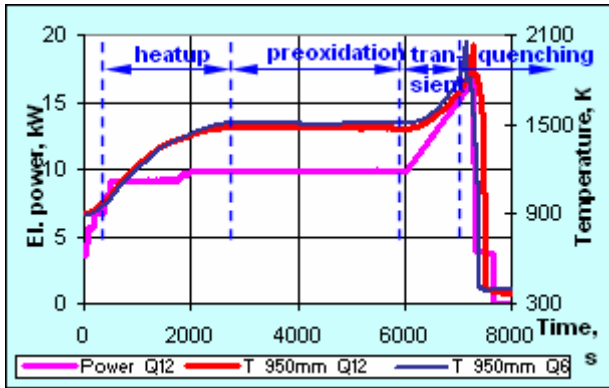


Fig. 12: Temperature at the 950 mm elevation and electric power vs. time together with an indication of test phases

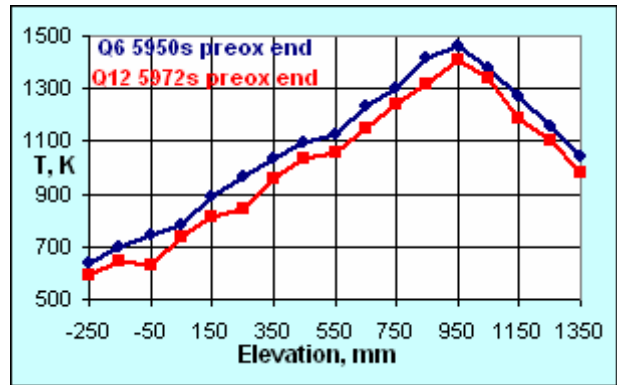


Fig. 13: Axial temperature distribution at the end of pre-oxidation phase

Corner rods withdrawn at the end of the pre-oxidation phase (rod D) and during the transient phase before quench initiation (rod F) revealed an extensive breakaway oxidation along the complete hot zone (Fig. 14).

The QUENCH-12 bundle was investigated in detail by videoscope (Fig. 15) before filling it with epoxy resin and by metallographic examination (Fig. 16). Axial differences in the surface morphology were observed. The lowest elevation where breakaway oxidation of cladding surface took place was at 400 mm. The maximum temperature at this bundle position was about 1120 K. No influence of the breakaway effect was observed for the QUENCH-06 bundle (Fig. 16). At the QUENCH-12 bundle, at the peak temperature elevation of 950 mm melt pool formation, non-coherent melt relocation, dissolution of embedded oxide scale and melt oxidation were observed.



Fig. 14: QUENCH-12, the withdrawn solid corner rods D and F (E110) revealed breakaway oxidation with intensive spalling of oxide scales



Fig. 15: QUENCH-12, videoscope inspection of breakaway effect at the 650 mm elevation. Cladding: E110, shroud: E125 alloy

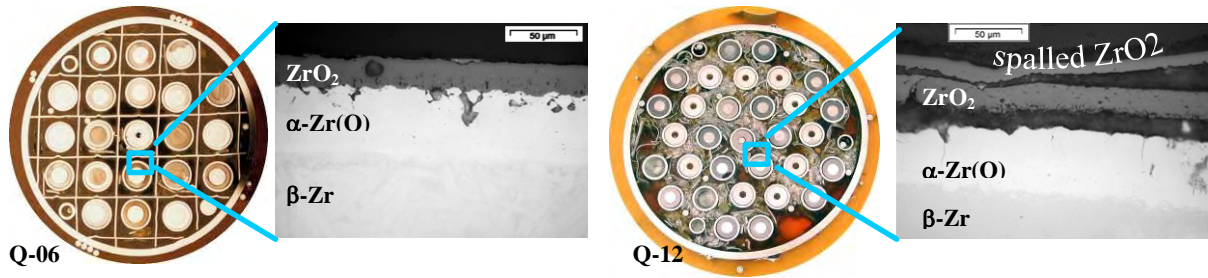


Fig. 16: Comparison of cross-sections of the QUENCH-06 and QUENCH-12 bundles at the 550 mm elevation

Measurements of hydrogen production during the QUENCH-12 test are as follows: 34 g were released during the pre-oxidation and transient phases and about 24 g in the quench phase. The amount released in the quench phase is six times higher than that in QUENCH 06 with ~4 g (Fig. 17, left) [26, 27]. Intensive hydriding of the QUENCH-12 claddings was observed at elevations with strong oxide spalling (Fig. 17, right) [24]. The reasons for the increased hydrogen production may be extensive damaging of the shroud, cladding, and corner rod surfaces due to the breakaway oxidation, local melt formation with subsequent melt oxidation, and the release of hydrogen previously absorbed by the metal.

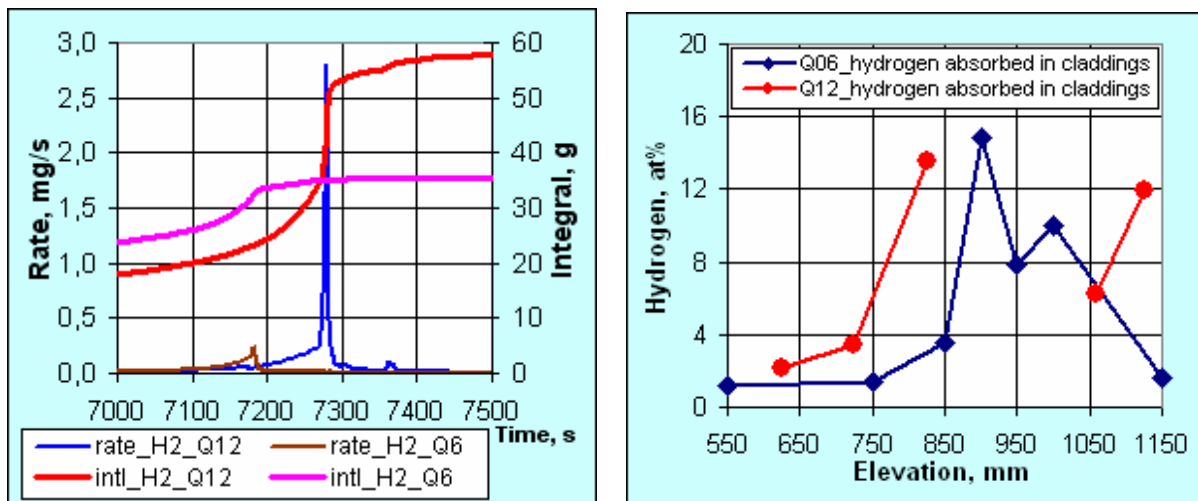


Fig. 17: Comparison of hydrogen production (left) and absorption (right) for the QUENCH-06 and QUENCH-12 tests

Analysis of QUENCH-12

A comparative assessment of QUENCH-06 and -12 provides an opportunity to examine the effect of alternative oxidation correlations on heat-up and hydrogen generation. Post-test calculations were performed using PSI (Paul-Scherrer-Institut) versions of SCDAP/RELAP5, following on from pre-test analyses [28] in support of the test definition. The input model was evolved from analyses of previous QUENCH tests with changes to accommodate the QUENCH-12 bundle configuration. Calculations were performed using the Sokolov correlation [29] for Zr1%Nb (E110) and two models for oxidation of Zry-4, namely the Cathcart-Pawel (C-P) correlation at $T < 1850$ K combined with (i) the Urbanic-Heidrick (U-H)

and (ii) the Prater-Courtright (P-C) correlation in the form recommended by Schanz et al. [30] at higher temperatures.

Fig. 18 compares the results using the three correlations with the measured temperatures at the hottest elevation (950 mm) of the central rod. All of the cases are close to the data during the plateau, with almost perfect agreement with the E110 correlation and only a very slightly higher temperature with Cathcart-Pawel. The E110 correlation leads to a sharper increase than U-H during the transient phase just before quench initiation, but with little impact on the temperature at that time. P-C gives a large overestimate in temperature just prior to quench. However, all three cases exhibit rapid cooling and quenching at almost the same time.

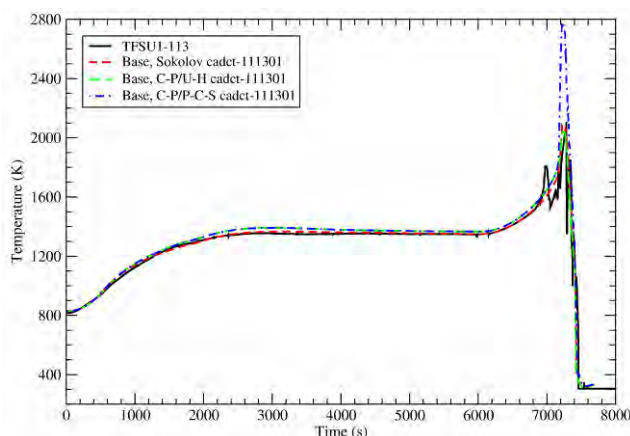


Fig. 18: Temperature at 0.95 m elevation on central rod

Despite the similar thermal response through almost the entire sequence, all of the calculations underestimated the oxidation, as can be seen in Fig. 19. The E110 correlation gives a much lower hydrogen generation during the plateau phase of the experiment, although the final mass is similar to the C-P/U-H case due to greater oxidation just before and during quench. The C-P/P-C correlation gives the closest agreement for hydrogen mass, including a significant oxidation during quench, but the rate is overestimated in the period just before while the total mass is still underestimated overall.

Although the E110 correlation gives a lower oxidation rate than C-P/U-H, the oxide thickness is greater. In fact the correlations for oxidation rate and oxide thickness are derived separately from weight gain and scale thickness measurements. The thicker oxide scale calculated by the E110 correlation suggests an inconsistency with the oxidised mass, or else evidence of a very low oxide density. Even so, Fig. 20 shows an underestimate over most of the oxidised length. It should be remembered that the QUENCH-12 behaviour suggests that E110 cladding may be prone to breakaway, suggesting that accurate measurements of weight gain and thickness might be difficult to obtain.

It is worthwhile to consider the calculated oxidation in relation to a comparison between QUENCH-06 and QUENCH-12. As indicated above the pre-quench phases of QUENCH-12 yielded 34 g, compared with 32 g in QUENCH-06. The effect of cladding material cannot be assessed by directly comparing the QUENCH-06 and QUENCH-12 results, partly because of the greater oxidisable surface area in QUENCH-12 (*1.22), and partly because the pre-oxidation plateau temperatures were up to 100 K lower in QUENCH-12. After taking into account the area ratio, the pre-quench oxidation in QUENCH-12 is only slightly less than QUENCH-06, despite the lower temperatures. In fact, although analyses of QUENCH-06 [25, 30] showed the C-P correlation to give quite good agreement for the pre-quench hydrogen generation, both the Sokolov and C-P correlation give an underestimate for QUENCH-12.

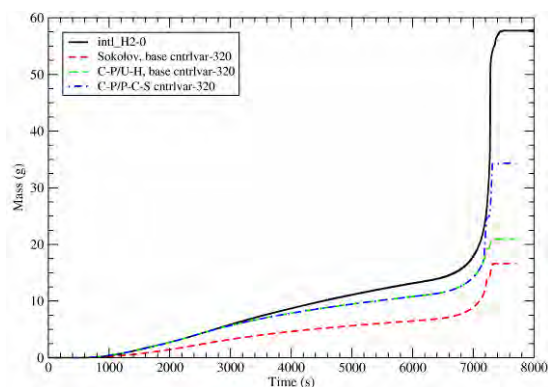


Fig. 19: Calculated and measured hydrogen generation

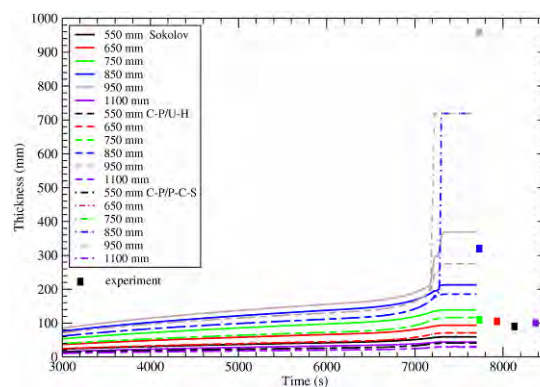


Fig. 20: Calculated and measured oxide scale thickness

These considerations suggest that under QUENCH-12 conditions the E110 cladding may be more susceptible to oxidation than Zry-4, as could also be expected from the observed breakaway. The quench phase of QUENCH-12 yielded 24 g of hydrogen, which was much more than in QUENCH-06. The correlations all significantly underestimate the quench oxidation in QUENCH-12, even the C-P/P-C model which strongly overestimated both the oxidation kinetics and the temperatures just before the start of quench. The differences between the correlations therefore do not explain the much greater hydrogen generation. Instead it appears this was due to processes outside the frame of a parabolic kinetic treatment, which enhanced the oxidation in QUENCH-12 but did not occur in QUENCH-06. Indeed, the QUENCH experiments have shown that hydrogen generation during reflood is a strong cliff-edge effect, triggered by various possible factors including the onset of metallic melting. A recent analysis by Vasiliev [31] identifies a number of factors that may have contributed to the reflood oxidation during QUENCH-12. Faster kinetics at temperatures above 1600 °C or more extensive shattering of the oxide scale cannot be ruled out. However, the analysis indicates that the metallic melting observed at some locations may be a more likely cause.

B.3.2 PARAMETER tests

At the PARAMETER test facility at SRI SIA “Luch” in the framework of the ISTC Project 1648.2 two experiments were performed to study the behaviour of VVER test assemblies under severe accident conditions aimed at cooling the overheated core by top and bottom flooding of the overheated test bundle.

The assembly was made up of 29 VVER fuel rod simulators together with standard reactor structural materials (Zr1Nb fuel rod claddings, UO₂ fuel pellets, Zr1Nb spacer grids, and shroud).

The scenario of the experiment included heat-up to temperature of ~1200 °C in the hottest zone in a mixture of flowing steam-argon, pre-oxidation of the assembly to reduce the effect of zirconium oxidation on the following heat-up and finally quenching with water (top flooding in the PARAMETER-SF1 experiment and combined flooding in the PARAMETER-SF2 test).

Responses of thermocouples attached at the fuel rod claddings at the elevations of 500-1300 mm in the PARAMETER-SF1 experiment are presented in Fig. 21. Post-test studies revealed the destruction of the test assembly at the elevations 700-1200 mm, i.e. the solidified melt

filled the coolant flow area practically completely at the elevations of 700-800 mm. In the course of top flooding the quick cooling (during 3-5 s) of the top elevations (1250-1500 mm) took place. Cooling of the bottom elevations 0-600 mm occurred much later for 400-600 s; the cooling front moved upwards. In the course of the experiment 91 g hydrogen were produced; the main portion of hydrogen (~59%) was released during flooding.

In the second experiment PARAMETER-SF2 no extra hydrogen release was recorded during the flooding of the test assembly. The main cause might be an absence of melt in the test assembly which was quenched as soon as the temperature of 1470 °C had been reached. In Fig. 22 readings of thermocouples fixed at the fuel rod claddings at the elevations of 500-1300 mm are presented for experiment PARAMETER-SF2.

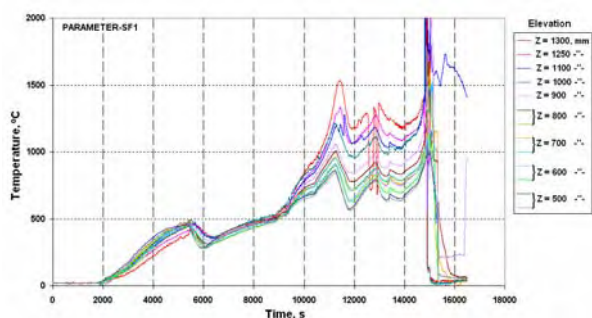


Fig. 21: PARAMETER-SF1. Indications of thermocouples on the fuel rod claddings at the elevations of 500-1300 mm

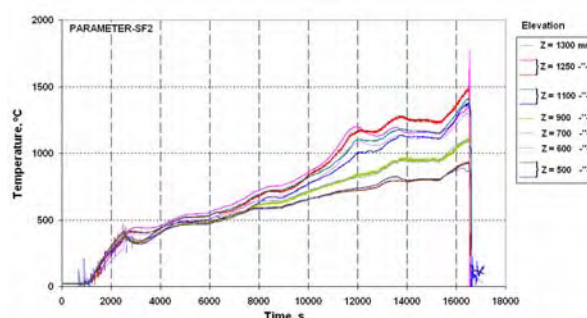
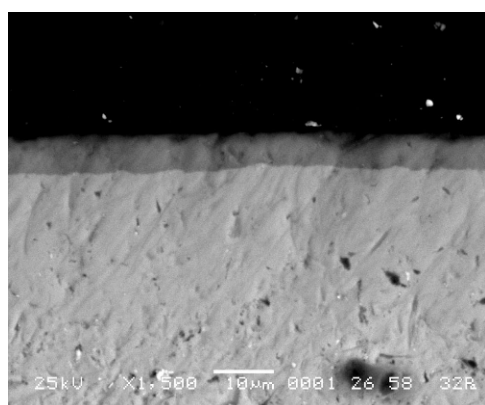
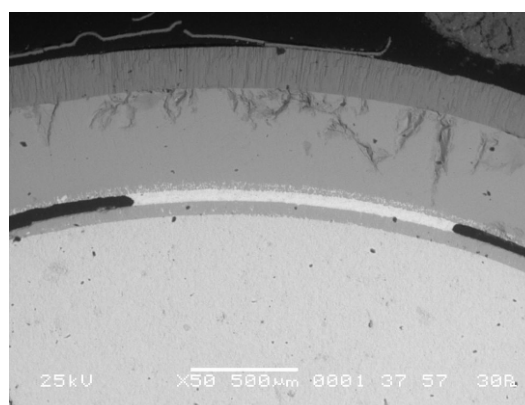


Fig. 22: PARAMETER-SF2. Indications of thermocouples on the fuel rod claddings at the elevations 500-1300 mm

Material investigations revealed zirconium dioxide on the metal surface of claddings well connected with metal and partially fragmented into sub-layers on the outside surface at elevations above 500 mm. Its thickness varies over the length of the test assembly reaching the maximum value at the elevation of 1200-1300 mm. The multi-layered spalling of the oxide scale was found on the outside surface of claddings as well due to long-term exposure of the bundle within the temperature range of 800-1100°C. At this range breakaway oxidation takes place in alloy E110 [6], as well as subsequently unsteady thermal loadings during combined flooding.



Z = 536 mm, fuel rod 3.12



Z = 1263 mm, fuel rod 3.12

Fig. 23: PARAMETER-SF1. Structure of oxide layers on the surface of fuel rod claddings

In the PARAMETER-SF1 experiment the major part of the area, where the layered oxide structure could be expected, melted off. Oxide layers remained at the elevations below 700 mm and above 1250 mm. At these elevations the formation of layered oxides was not strongly pronounced in PARAMETER-SF1. In Fig. 23 the structure of oxide layers on fuel rod claddings is shown for the elevations of 536 and 1263 mm.

B.3.3 CODEX tests with special emphasis on cladding behaviour

The CODEX (Core Degradation Experiment) experimental program included four tests with quenching VVER fuel rods from high temperature. The CODEX-3/1 and 3/2 experiments simulated the behaviour of fuel rods in reactor accidents, while the CODEX-CT-1 and CT-2 described the main conditions of the Paks-2 cleaning tank incident. In all tests 1 m long electrically heated 7-rod bundles were applied. In the CODEX-3/1 and 3/2 test uranium pellets were used and tungsten heaters were inside the rods. In the CODEX-CT-1 and CT-2 tests alumina pellets were placed in the fuel rod simulators and external heaters produced the necessary thermal conditions.

The main purpose of the CODEX-3/1 and CODEX-3/2 tests was to investigate the effect of water quenching on the degradation process of a VVER bundle [32]. It was expected to receive similar results as in the CORA tests for PWR and BWR bundles, where the initiation of quenching led to temperature excursion and high hydrogen production. The differences in the bundle geometry and core materials were to be evaluated. In both experiments water quenching was applied as a cooling-down process after high-temperature oxidation of the bundle. However, the temperatures and the initial bundle states were different in the two cases. These parameters had an important effect on the final bundle states and the degree of degradation.

In the CODEX-3/1 test the maximum temperature at the upper part of the facility reached 1150 °C (Fig. 24). It took about 90 s to quench the total heated length of the bundle from the bottom and the facility rapidly cooled down. This test showed only a very limited temperature excursion of about 10 K after initiating the quench. Furthermore the later investigation showed that during this rapid cooling-down process the fuel integrity was maintained. For the oxide layer thickness a post-test calculation estimated 50 µm in the hottest part of the bundle. The visual examination showed no cracks in the oxide layer.

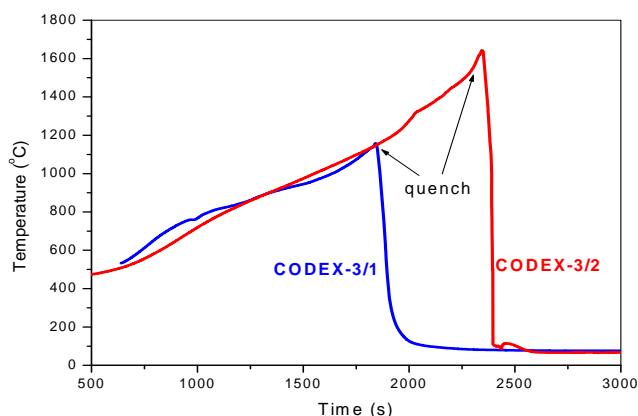


Fig. 24: Temperature histories of CODEX-3/1 and CODEX-3/2 tests

The CODEX-3/2 quench test was carried out with the same bundle, which was pre-oxidized in the CODEX-3/1 experiment. Water quenching was initiated when the maximum temperature reached 1500 °C (Fig. 24). The duration of quenching was about 80 s. Water

injection produced some temperature excursion, but the maximum temperature increase was less than 200 K and the maximum temperature remained below 1700 °C. The post-test examination of the bundle showed signs of high-temperature interaction between UO₂ pellet and Zr cladding (Fig. 25). The oxide layer on both internal and external sides of the cladding was compact. The main conclusion from the CODEX-3/2 experiment was that the oxide layer on the external surface of the cladding could play a protective role during water quenching and to some extent could limit the cladding oxidation, hydrogen production and, thus, the degradation process. Similarly, in the QUENCH-01 test performed at FZK with a bundle moderately pre-oxidized, reflooding took place smoothly with no evidence of temperature excursion or excess hydrogen production [33]. This fact confirmed that the reason for the unexpected behaviour of the CODEX-3/2 bundle during quenching was not the material and geometry of VVER fuel, but the protective role of the oxide layer on the external surface of cladding.

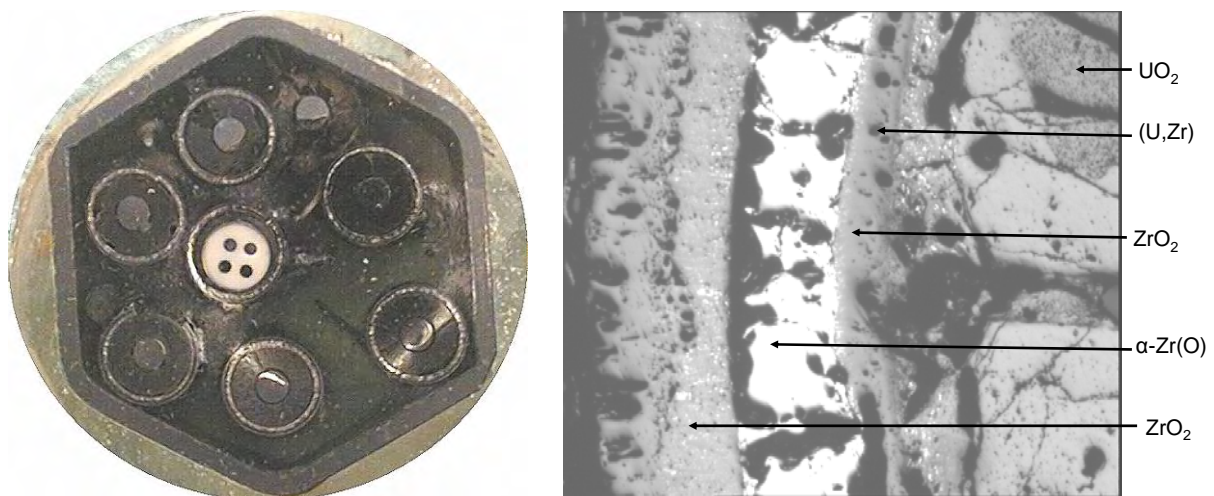


Fig. 25: Cross section of CODEX-3 bundle (left) and details of cladding structure (right)

The cleaning tank incident at the unit 2 of the Paks NPP in 2003 resulted in severe fuel damage of 30 assemblies [34]. The fuel rods heated up due to insufficient cooling and the zirconium components suffered heavy oxidation. Opening of the tank and quenching of the assemblies by cold water led to fragmentation of the brittle zirconium components.

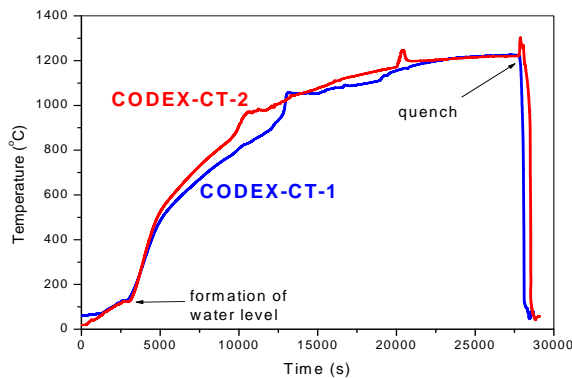


Fig. 26: Temperature histories of CODEX-CT-1 and CODEX-CT-2 tests

In order to improve the understanding of the phenomena that took place during the Paks-2 incident integral tests have been carried out in the CODEX facility. The tests simulated the

whole scenario of the incident including the water quench. The final state of the fuel rods showed many similarities with the conditions observed after the incident at the NPP and for this reason it is very probable that the thermal conditions and chemical reactions were also similar in the tests and in the incident. The main boundary conditions were similar for the CODEX-CT-1 and CODEX-CT-2 tests. The most significant difference between the two tests was the operation of the air let-down valve that was open in the first test and closed in the second one. In the second test the hydrogen produced in the Zr-steam reaction could not escape from the test section and it prevented the access of steam to the Zr surfaces and caused much less oxidation than in the first tests. The final quench by water resulted in smooth cool down in the CODEX-CT-1 test and led to a temperature excursion in the CODEX-CT-2 bundle (Fig. 26). The final state of the bundles was very brittle, the fuel rods and the shrouds were cracked and fragmented (Fig. 27). The post-test examination of CODEX-CT-1 and CT-2 bundles indicated that the high degree of embrittlement was a common result of oxidation and hydrogen uptake by the Zr components. The oxide scale had fine layered structure and the metallic phase absorbed a large amount of hydrogen (Fig. 27). Both tests were carried out in hydrogen-rich steam atmosphere. The high hydrogen content of steam led to slower oxidation reaction, but the uptake of hydrogen by Zr was very high.



Fig. 27: Cross section of CODEX-CT-2 bundle (left) and piece of cladding with layered oxide scale (right)

The different structure of oxide scale observed in CODEX-3/2 and CODEX-CT-2 test can be explained by the temperature histories (Table 2). In case of CODEX-3/2 the temperature increase was fast and most of the oxidation took place well above 1200 °C. This resulted in a compact oxide scale. The temperature increase was much slower in the CODEX-CT-2 test and most the oxidation process happened between 1000-1200 °C. These conditions produced layered oxide scale showing the breakaway effect.

Table 2: Comparison of main parameters of the CODEX VVER quench tests.

Parameter	CODEX-3/1	CODEX-3/2	CODEX-CT-1	CODEX-CT-2
Oxidation time above 600 °C (s)	1153	1570	21666	22724
Max. temperature before quench (°C)	1150	1500	1245	1286
Max. temperature during quench (°C)	1158	1643	1245	1384
Total hydrogen production (g)	0.1	1	33	13

C Status of modelling

C.1 Oxidation kinetics

High-temperature steam oxidation kinetics of solid Zircaloy are modelled in both system-level and detailed codes (e.g. MELCOR and ICARE2, respectively), typically assuming parabolic kinetics with parameters developed by, for example, Urbanic and Heidrick [35]. These parameter values appear to the code users to be adequate as long as the Zircaloy is solid. However, more recent work performed in the frame of the COLOSS project [36] resulted in the recommendation of alternative, arguably better correlations [11], namely Leistikow (at $T < 1550^\circ\text{C}$) and Prater-Courtright (at $T > 1550^\circ\text{C}$). These recommendations were essentially based on a thorough analysis of available oxidation kinetic results with respect to their reliability and statistical methods of evaluating the data sets, documented in [37, 19]. The work was performed to support development of the detailed SVECHA/QUENCH (S/Q) code within the bilateral FZK-IBRAE collaboration. Best-estimate diffusion coefficients for ZrO_2 , $\alpha\text{-Zr(O)}$ and $\beta\text{-Zr}$ were deduced from this analysis for the temperature range 1273 to 1773 K and the diffusion coefficient of cubic ZrO_2 for the temperature range 1798 to 2098 K. The thus determined best-estimate diffusion coefficients were successfully validated in [19] against temperature transient tests [38, 39].

A similar procedure of diffusion coefficient determination was performed for Zr1%Nb alloy (E110) [19] on the base of the test data from RIAR [5]. Results of these calculations are presented in the same graphs, Fig. 28, for direct comparison of the two materials.

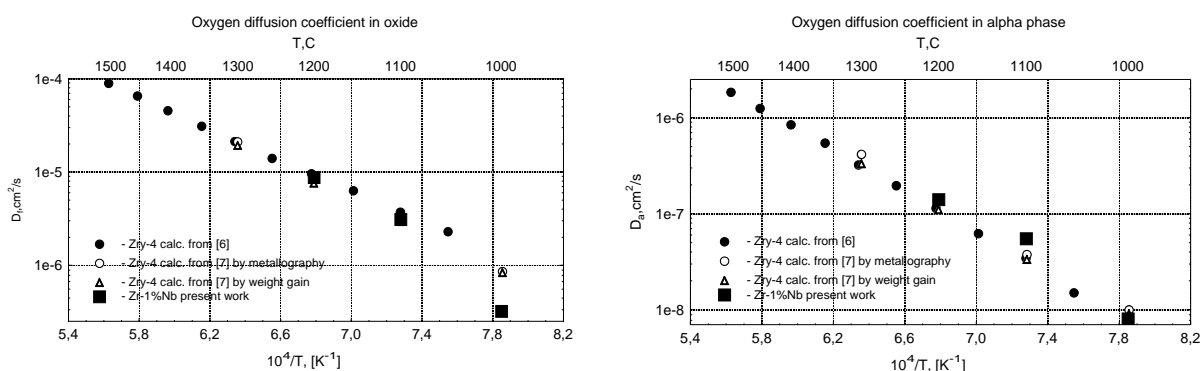


Fig. 28: Calculated oxygen diffusion coefficients in ZrO_2 and $\alpha\text{-Zr(O)}$ for Zr1%Nb and Zry-4

The various kinetic correlations derived from experimental data in the past are summarised in Tables 3, 4 and Fig. 29. An evaluative analysis for E110 data (comparable to Schanz' work) is not yet available. The most recent data for E110 have been obtained by Grosse [7], see also chapter 2.1.2.

Table 3 describes the oxide layer thickness growth $\delta^2 = K_t \cdot t$ with rate coefficient $K_t = K_{0t} \cdot e^{-T_e/T}$ and Table 4 the weight gain during oxidation $w^2 = K_w \cdot t$ with rate coefficient $K_w = K_{0wt} \cdot e^{-T_w/T}$. The presented correlations for Zircaloy-4 are described in [11, 19], wherein the best-fitted correlations for Zry-4 recommended by Schanz are marked with colour. All experiments were performed with double-sided oxidation of samples.

Table 3: Parameters of different correlations for oxide thickness growth for Zry-4 and E110.

Alloy	Kinetic	Temperature range, °C	Oxidation degree, μm	K_{Ot} , cm^2/s	T_{et} , K
Zry-4	UH (AECL, 1978)	1580-1850	$\delta_{ox} > 200$	$2 \cdot 10^{-2}$	16014
Zry-4	PC (PNNL, 1986)	1630-2000	$100 < \delta_{ox} < 600$	$2981.16 \cdot 10^{-2}$	28420
Zry-4	CP (ORNL, 1979)	1000-1500	$\delta_{ox} < 75$	$2.252 \cdot 10^{-2}$	18062
Zry-4	LS (FZK, 1983) [38]	900-1500	$\delta_{ox} < 600$	$7.82 \cdot 10^{-2}$	20214
Zry-4	FZK, 2006	1050-1400	$50 < \delta_{ox} < 550$	$6.64 \cdot 10^{-2}$	19121
E110	RIAR, 1981 [4]	350-600	$\delta_{ox} < 100$	$6.45 \cdot 10^{-2}$	20242
E110	VNIINM, 1993 [29]	1000-1500	$\delta_{ox} < 100$	$0.519 \cdot 10^{-2}$	15355
E110	VNIINM, 1993 [29]	1500-1600	$\delta_{ox} < 150$	$1.772 \cdot 10^{-2}$	14680
E110	VV, 1993 [42]	600-1450	$\delta_{ox} < 250$	$3.13 \cdot 10^{-2}$	19382
E110	AEKI, 2003 [47]	500-1200	$\delta_{ox} < 150$	$16 \cdot 10^{-2}$	20400
E110	FZK, 2006	1050-1400	$50 < \delta_{ox} < 350$	$132 \cdot 10^{-2}$	24140

Table 4: Parameters of different correlations for weight gain for Zry-4 and E110.

Alloy	Kinetic	Temperature range, °C	Oxidation degree, μm	K_{Ow} , ($\text{g}^2/\text{cm}^4\text{s}$)	T_{ew} , K
Zry-4	UH (AECL, 1978)	1580-1850	$\delta_{ox} > 200$	0.879	16610
Zry-4	PC (PNNL, 1986)	1630-2000	$100 < \delta_{ox} < 600$	32.95	26440
Zry-4	CP (ORNL, 1979)	1000-1500	$\delta_{ox} < 75$	0.3622	20100
Zry-4	LS (FZK, 1983) [38]	900-1500	$\delta_{ox} < 600$	0.52418	20962
Zry-4	FZK, 2006	1050-1400	$50 < \delta_{ox} < 550$	0.0888	18067
E110	RIAR, 1981 [4]	350-600	$\delta_{ox} < 100$	0.8464	20820
E110	VNIINM, 1993 [29]	1000-1500	$\delta_{ox} < 100$	1.59	23040
E110	VNIINM, 1993 [29]	1500-1600	$\delta_{ox} < 150$	0.9825	20800
E110	VV, 1993 [42]	600-1450	$\delta_{ox} < 250$	0.561	21426
E110	BDL (FZR) [3]	700-1100	$\delta_{ox} < 100$	0.2375	20522
E110	KI/RIAR, 2005 [5]	800-1200	$\delta_{ox} < 100$	0.09772	19105
E110	AEKI, 2003 [47]	500-1200	$\delta_{ox} < 150$	0.4330	20400
E110	FZK, 2006	1050-1400	$50 < \delta_{ox} < 350$	1.5952	22664

The following abbreviations applied are above: UH – Urbanic, Heidrick; PC – Prater, Courtright; CP – Cathcart, Pawel; LS – Leistikow, Schanz, VV- Vrtilkova, Valach, BDL – Böhmert, Dietrich, Linek;

FZK data were obtained by Grosse, VNIINM data by Sokolov.

δ_{ox} – oxide layer thickness.

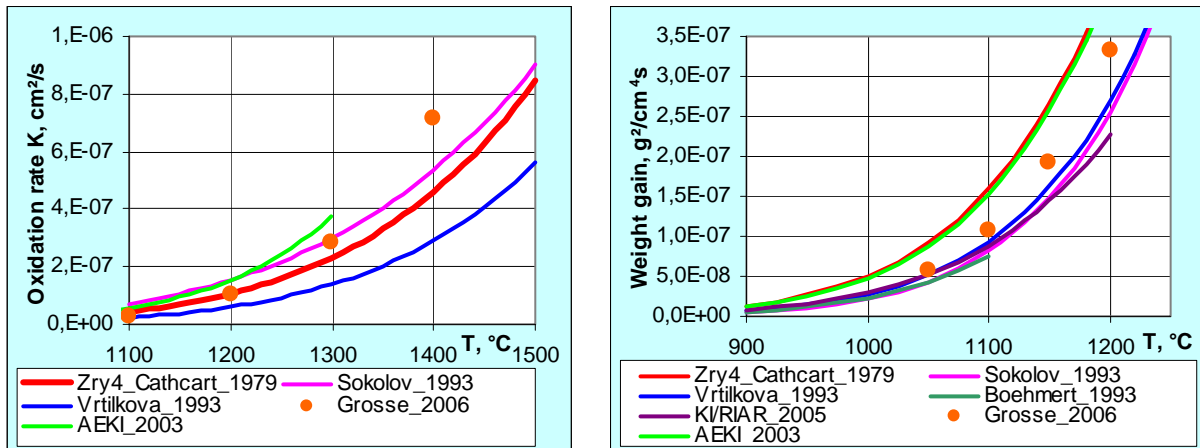


Fig. 29: Comparison of different correlations for growth of oxide layer (left) and weight gain (right) during E110 cladding oxidation. The CP correlation for Zry-4 is used as reference.

In Fig. 29 (right) all but the AEKI weight gain correlations for E110 oxidation are similar to each other (within this relatively close temperature range) and are less than CP correlation for Zry-4. This trend is confirmed by the recent FZK single-effect tests (chapter B.1.2), which showed a lower oxidation rate for the E110 in comparison to Zry-4 in temperature range between 1050 °C and 1400 °C. Thus the Vrtilkova and Sokolov correlations for weight gain almost coincide. However growth of the oxide layer is determined very differently by Vrtilkova and Sokolov. In general there is significant scattering among the E110 oxide layer growth correlations proposed by the different authors. This variation suggests some basic uncertainty which should be investigated further. Possible causes may be the use of different sets of test cases, or different assumptions concerning the thickness of metal (finite or semi-infinite).

C.2 Thermo-mechanical behaviour during cool-down

The Mechanical Deformation model of the S/Q code was developed to predict the deformation and rupture behaviour of Zircaloy fuel cladding under severe accident conditions [19]. In this approach during quenching of the oxidized fuel cladding tensile stress is generated in the oxide due to the radial temperature gradient and the difference in the thermal strains of the α -phase, β -phase and oxide layers. This tensile stress leads to the onset of micro-cracks in the oxide scale at temperatures above the tetragonal-to-monoclinic phase transition (Fig. 30, left, from [46]).

At temperatures below the tetragonal-to-monoclinic phase transition (attained during quenching) the high compressive stress occurs in the oxide layer and the high tensile stress – in the alpha layer. Low oxygen content in the metal β -layer is the main reason for a prevention of through-wall crack formation. In this case the Chung-Kassner criterion [40] can be applied: to withstand a thermal shock during quenching the thickness of the cladding with ≤ 0.9 wt% oxygen should be greater than 0.1 mm. If this layer is thinner and additionally the oxide scale with the residual deformation strength is thick enough to generate in the α -layer the stress exceeding the tensile limit, then the through-wall cracks appear. Otherwise micro-cracks appear in the oxide scale (Fig. 30, right). Oxide micro-cracking and creep strain in the metal layers lead to the relaxation of high level stresses.

The developed approach to the through-wall crack density evaluation furnishes a satisfactory agreement with experimental data of the FZK quench rig tests on the through-wall crack formation in dependence on initial quenching temperature and pre-oxidation of the cladding [21].

The S/Q code was adapted to simulate thermo-mechanical behaviour and failure of the VVER fuel rod simulators in the new RIAR quench tests, using the material data base for E110 alloy. The modified S/Q code well predicts the temperature evolution during quenching, the maximum extent of Zr1%Nb cladding oxidation and the final mechanical state of the oxidized Zr1%Nb cladding in the tests with fresh uranium fuel rods. The predictions are in good agreement with results of the FZK quench rig tests (with Zry-4 cladding).

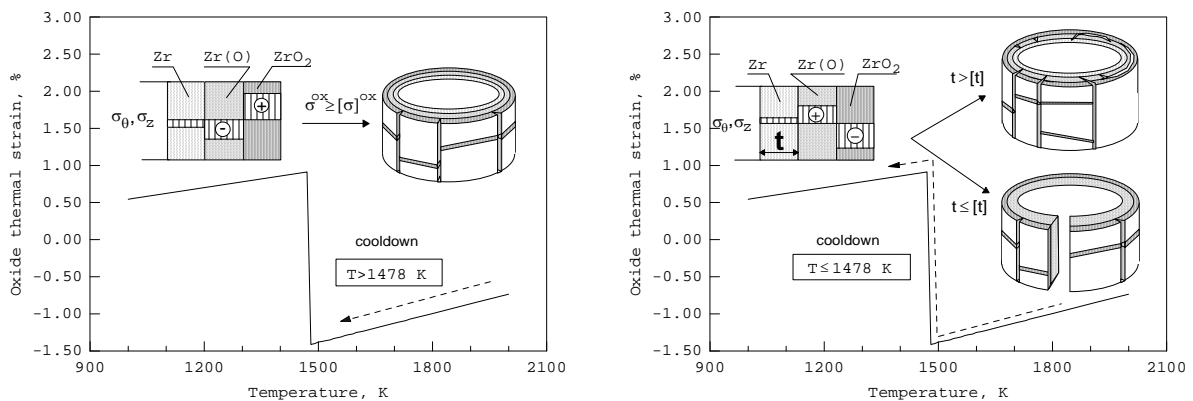


Fig. 30: Scheme of the stress state and failure modes of oxidized cladding on cool-down above the oxide phase transition temperature (left) and below the oxide phase transition temperature (right) (from [46]).

C.3 Influence of irradiation

At IBRAE the S/Q code was further extended for simulation of the RIAR quench tests with irradiated fuel rods (ISTC Project #1648.2). First of all, calculations of the S/Q code confirm observations of complete disappearance of a gap between fuel pellets and cladding at operation temperatures for high burnup. In this case S/Q predicts chemical interactions of zirconium cladding with uranium dioxide that result in formation of internal α -Zr(O) layer and, following to the earlier FZK separate-effect tests observations [41], embrittlement of the cladding. Thus, the fuel rod cladding embrittlement can take place even lacking external oxidation. Basing on the Chung-Kassner criterion (for handling), for such test conditions the S/Q code correctly predicts fuel rods failure during handling after the test.

However, additional external cladding oxidation considerably enhances cladding embrittlement. Based on the Chung-Kassner criterion (for thermal shock) for such test conditions, the S/Q code predicts fuel rod failure during quenching. Detailed thermo-mechanical consideration of the S/Q code predictions confirms this conclusion and demonstrates formation of through-wall cracks in fuel rods during quenching, owing to high tensile stresses induced by the fuel pellet in both α -Zr(O) and oxide layers of the cladding. This essentially reduces conservatism of the Chung-Kassner criterions (in comparison with the case of unirradiated fuel rods).

D Conclusions and outlook

The paper summarised the publicly available information on high-temperature behaviour of Zircaloy-4 and E110 with the focus on the more recent experiments and model development. Small-scale separate-effects tests, single-rod experiments as well as various bundle experiments have been considered. Meanwhile a considerable data base of high-temperature behaviour is available for both alloys which allows drawing some general conclusions.

Both alloys behave similar at temperatures above and including 1100 °C, where breakaway oxidation plays no role. Maximum differences in oxidation rates of about 20 % have been observed in this region with slightly lower oxidation rates of E110 up to ca. 1350 °C and inverted behaviour at higher temperatures. The oxidation rates of both alloys clearly reflect the phase changes of the superficial zirconia layer from monoclinic to tetragonal and cubic. Increasing sub-stoichiometry, i.e. increasing x in the formula ZrO_{2-x} , cause a rise in oxygen diffusion coefficients and therefore oxidation rates.

Significant differences between the alloys have been observed in the temperature range 600-1050 °C. The susceptibility to breakaway oxidation, i.e. the formation of layered and cracked oxide scales, which are not anymore completely protective, strongly depends on temperature. At lower temperatures (600-700 °C) long-term oxidation tests revealed a beneficial behaviour of E110. At ca. 800-900 °C very pronounced breakaway led to strong degradation of E110 cladding, whereas at 1000 °C breakaway of Zircaloy-4 was stronger. Generally, breakaway causes the transition from parabolic (or cubic at lower temperatures) oxidation kinetics to faster, more linear kinetics. Local enrichment of hydrogen leads to much higher absorption of hydrogen by the remaining metal than expected from the global hydrogen partial pressure in the atmosphere. Furthermore, the oxidation in air is strongly influenced by the breakaway effect, because diffusion of nitrogen through cracks to the metal-oxide boundary accelerated nitrogen attack and nitride formation.

Generally, E110 seems to be more susceptible to breakaway. Transient small-scale tests only for E110 resulted in temporary breakaway oxidation. Although the large scale bundle tests QUENCH-06 (Zry-4) and QUENCH-12 (E110) were not completely identical, breakaway and its consequences (hydrogen release and absorption) were more pronounced at QUENCH-12. The scenario of both tests with a long-term pre-oxidation phase is more relevant for spent fuel pool accidents than for reactor accidents. During this phase strong hydriding of the cladding during breakaway oxidation caused strong material embrittlement, which led to stronger degradation of the E110 bundle during quenching and higher hydrogen release. A similar sequence of events was observed during the Paks accident with a cleaning tank [34]. As a consequence, the production process of E110 will be changed soon from “electrolytic” to “metal sponge” method. The first results show better behaviour for the new cladding in high temperature conditions (compact oxide scale, less embrittlement). For this reason new test series should be carried out with the new E110.

Thanks to Veshchunov et al. [37] and Schanz et al. [2, 11, 30] for Zircaloy-4 a best-fitted correlation of the oxidation kinetics up to very high temperatures is available. Although various experimental data sets are available, a comparable analysis of the E110 data is still missing, and it is proposed to start a corresponding initiative as soon as possible.

The comparison of the two alloys Zircaloy-4 and E110 has shown that, although the differences in composition are small (>98 wt% Zr), the behaviour in the temperature region 600-1050 °C is significantly different. As new cladding materials, as M5, Duplex or Zirlo, are increasingly used in Europe and elsewhere, there is a clear need for further investigations

because the accident codes still almost exclusively rely on Zircaloy-4 data. The QUENCH-ACM (Advanced Cladding Materials) [43] programme including separate-effects and bundle tests with advanced cladding materials has already been launched at FZK. Other test atmospheres are considered in e.g. the PARAMETER programme with the SF4 experiments planned to be conducted including an air ingress phase.

References

- [1] B. Cox, "Some thoughts on the mechanisms of in-reactor corrosion of zirconium alloys", *J. Nucl. Mater.* 336 (2005), 331-368.
- [2] G. Schanz, B. Adroguer, A. Volchek, "Advanced treatment of Zircaloy cladding high-temperature oxidation in severe accident code calculations. Part I. Experimental database and basic modeling", *Nucl. Eng. Design* 232 (2004), 75-84.
- [3] J. Böhmert, M. Dietrich, J. Linek, "Comparative studies on high-temperature corrosion of ZrNb1 and Zircaloy-4", *Nucl. Eng. Design* 147 (1993), 53-62.
- [4] V.A. Tzikanov et al., Preprint NIIAR-32(485), Dimitrovgrad, 1981.
- [5] L. Yegorova, K. Lioutov, N. Jouravkova, A. Konobeev, V. Smirnov, V. Chesanov, A. Goryachev, "Experimental Study of Embrittlement of Zr-1%Nb VVER Cladding under LOCA-Relevant Conditions", Report NUREG/IA-021, IRSN 2005-194, NSI RRC KI 3188, NRC Washington, DC 20555-0001, March 2005.
- [6] Y.K. Bibilashvili, N.B. Sokolov, L.N. Andreyeva-Andrievskaya, A.V. Salatov, A.M. Morozov, "High-Temperature Interaction of Fuel Rod Cladding Materials (Zr1Nb Alloy) with Oxygen Containing Medium", IAEA-TECDOC-921, Dimitrovgrad, 1995.
- [7] M. Grosse, "Comparison of the high temperature oxidation behaviour of different cladding materials", *Jahrestagung Kerntechnik 2007*, Karlsruhe, 22-24 May 2007, Berlin, INFORUM GmbH, 285-288.
- [8] M. Steinbrück, "Oxidation of advanced zirconium alloys in oxygen in the temperature range 600-1600 °C", *Proc. of the 16th Int. Conf. Nucl. Eng. ICONE-16*, 11-15 May 2008, Orlando, Florida, paper 48054.
- [9] Z. Hózer, C. Györi, L. Matus, M. Horváth, "Ductile to brittle transition of oxidised Zircaloy-4 and E110 claddings", *J. Nucl. Mat.* 373 (2008), 415-423.
- [10] G. Hache, H.M. Chung, "The history of LOCA embrittlement criteria", *Proc. 28th Water Reactor Safety Information Meeting*, 23-25 October 2001, Bethesda, USA, NUREG/CP-0172, pp. 205-237.
- [11] G. Schanz, "Recommendations and Supporting Information on the Choice of Zirconium Oxidation Models in Severe Accident Codes", FZKA 6827, SAM-COLOSS-P043, 2003.
- [12] V. Vrtilkova, J. Vesely, "An Approach to the Alternative LOCA Embrittlement Criterion", *SEGFSM Topical Meeting on LOCA Issues*, ANL, USA, 25-26 May, 2004.
- [13] V.I.Solyany, Yu.K.Bibilashvili, V. Yu Tonkov., "High Temperature Oxidation and Deformation of Zr1%Nb Alloy of VVER Fuels", *Proc. of OECD-NEA-CSNI/IAEA Specialist Meeting on Water Reactor Fuel Safety and Fission Product Release in Off-Normal and Accident Conditions*, Riso (Denmark), 16-20 May, 1983.
- [14] E. Perez-Feró, Cs. Györi, L. Matus, L. Vasáros, Z. Hózer, P. Windberg, L. Maróti, M. Horváth, I. Nagy, A. Pintér-Csordás, T. Novotny, "Experimental Database of E110 Claddings under Accident Conditions", AEKI-FRL-2007-123-01/01, Budapest, 2007 (<http://www.nea.fr/abs/html/nea-1799.html>).
- [15] M. Steinbrück, C. Duriez, J. Birchley, T. Haste, D. Ohai, T. Meleg, "Separate-effects tests on zircaloy cladding degradation in air ingress situations", *2nd European Review Meeting on Severe Accident Research (ERMSAR-2007)*, Karlsruhe, June 12-14, 2007.

- [16] O. Coindreau et al., "Modelling and accelerated cladding deformation in air for severe accident codes", this conference, paper 2.4.
- [17] P. Giordano et al., "Ruthenium behaviour under air ingress conditions: main achievements in the SARNET project", this conference, paper 3.9.
- [18] N. Ver, "Determination of kinetic parameters of the oxidation of zirconium alloys in steam/air mixtures", AEKI-FRL-2007-401-01/01, Budapest, 2007.
- [19] P. Hofmann, V. Noack, M. S. Veshchunov, A. V. Berdyshev, A. V. Boldyrev L. V. Matweev, A. V. Palagin, "Physico-Chemical Behaviour of Zircaloy Fuel Rod Cladding Tubes During LWR Severe Accident Reflood. Part I: Experimental results of single rod quench experiments. Part II: Modelling of quench phenomena ", FZKA 5846, Karlsruhe, 1997.
- [20] L. Steinbock, J. Stuckert, "Determination of the crack pattern of quenched Zircaloy tubes", FZKA-6013, Karlsruhe, 1997.
- [21] P. Hofmann, A. Miassoedov, L. Steinbock, M. Steinbrück, A.V. Berdyshev, A.V. Boldyrev, A.V. Palagin, V.E. Shestak, M.S. Veshchunov, "Quench behaviour of Zircaloy fuel rod cladding tubes. Small-scale experiments and modelling of the quench phenomena", FZKA 6208, Karlsruhe, 1999.
- [22] J. Stuckert, M. Steinbrück, U. Stegmaier, "Single rod quench tests with Zr-1Nb cladding. Comparison with Zircaloy 4 cladding tests and modelling", FZKA 6604, Karlsruhe, June 2001.
- [23] J. Stuckert, L. Sepold, M. Steinbrück, "Results of the QUENCH-12 experiment on reflood of a VVER-type bundle", Jahrestagung Kerntechnik 2007, Karlsruhe, 22.-24.Mai 2007. Berlin: INFORUM GmbH, 2007. CD-ROM.
- [24] J. Stuckert et al., "Results of the QUENCH-12 Experiment on Reflood of a VVER-type Bundle", FZKA 7307, Karlsruhe, 2008.
- [25] L. Sepold, W. Hering, C. Homann, A. Miassoedov, G. Schanz, U. Stegmaier, M. Steinbrück, H. Steiner, J. Stuckert, "Experimental and Computational Results of the QUENCH-06 Test (OECD ISP-45)", FZKA 6664, Karlsruhe, 2004.
- [26] M. Grosse, M. Steinbrueck, E. Lehmann, P. Vontobel, "Kinetics of Hydrogen Absorption and Release in Zirconium Alloys During Steam Oxidation", Oxid Met DOI 10.1007/s11085-008-9113-2, 2008
- [27] M Grosse, G Kuehne, M Steinbrueck, E Lehmann, J Stuckert, and P Vontobel, "Quantification of hydrogen uptake of steam-oxidized zirconium alloys by means of neutron radiography", Journal of Physics: Condensed Matter, **20** (2008) 104263 (7pp)
- [28] J. Birchley, T. Haste, W. Hering and C. Homann, "Pre-test Analytical Support for Experiments QUENCH-10, -11 and -12", Int. Conf. Nuclear Energy for New Europe 2006, Portorož, Slovenia 2006.
- [29] N. B. Sokolov, L. N. Andreeva-Andrievska, V. Yu. Vlasov et al., "Genetics of the Interaction of VVER Reactor Core Materials – Recommendations for Use on the Basis of the International Standard Problem on the CORA-W2 Experiment", A A Bochvar All-Russian Scientific Research Institute for Inorganic Materials (VNIINM) Report N8068, Moscow, Russia 1993.
- [30] A. Volchek, Y. Zvonarev and G. Schanz, "Advanced Treatment of Zircaloy Cladding High Temperature Oxidation in Severe Accident Calculations Part II. Best-fitted parabolic correlations", Nuc. Eng. Des. 232, 85-96 2004.
- [31] A. Vasiliev, "QUENCH-12 versus QUENCH-06 Comparative Calculation Analysis using SOCRAT 1.1 Code", 13th Int. QUENCH Workshop, FZ Karlsruhe, Germany, 2007.
- [32] Z. Hózer, L. Maróti, P. Windberg, L. Matus, I. Nagy, Gy. Gyenes, M. Horváth, A. Pintér, M. Balaskó, A. Czitrovsky, P. Jani, A. Nagy, O. Prokopiev, B. Tóth, "Behavior of VVER fuel rods tested under severe accident conditions in the CODEX facility", Nuclear Technology 154 (2006), 203-317.
- [33] P. Hofmann, W. Hering, C. Homann, W. Leiling, A. Miassoedov, D. Piel, L. Schmidt, L. Sepold and M. Steinbrück, "QUENCH-01 Experimental and Computational Results", FZKA 6100, Forschungszentrum Karlsruhe, 1998.

- [34] Final Report of the OECD-IAEA Paks Fuel Project NEA/CSNI/R(2008)2 (restricted).
- [35] V.F. Urbanic, T.R. Heidrick, "High-temperature oxidation of Zircaloy-2 and Zircaloy-4 in steam", J. Nucl. Mater. 75 (1978), 251-261.
- [36] B. Adroguer et al., "Core loss during a severe accident (COLOSS)", Nuclear Engineering and Design, 235 (2005), 173-98.
- [37] A.V. Berdyshev, L.V. Matveev, M.S. Veshchunov, "Development of the data base for the kinetic model of the Zircaloy4/steam oxidation at high temperatures ($1000^{\circ}\text{C} \leq T \leq 1825^{\circ}\text{C}$)", Russian Academy of Sciences, Nuclear Safety Institute, IBRAE-97-05, Moscow, 1997.
- [38] S. Leistikow, G. Schanz. "Oxidation kinetics and related phenomena of Zircaloy-4 fuel cladding exposed to high temperature steam and hydrogen-steam mixtures under PWR accident conditions", Nuclear Engineering and Design, 1987, v.103, N 1, pp. 65-84.
- [39] P. Hofmann, H.J. Neitzel, "Experimental and Theoretical Results of Cladding Oxidation under Severe Fuel-Damage Conditions" / Zirconium in the Nuclear Industry: Seventh International Symposium, ASTM STP 939, R.B. Adamson and L.F.P. Van Swan, Eds., American Society for Testing and Materials, Philadelphia, 1987, 504-538.
- [40] H.M. Chung, T.F. Kassner, "Embrittlement Criteria for Zircaloy Fuel Cladding Applicable to Accident Situations in Light-Water Reactor: Summary Report", Argonne National Laboratory, Materials Science Division, NUREG/CR-1344, ANL-79-48, 1980.
- [41] P. Hofmann, "Chemical Interactions of Zircaloy-4 Tubing with UO_2 Fuel and Oxygen at Temperatures between 900 and 2000°C (Experiments and PECLOX Code), Part I: Experimental Results", Kernforschungszentrum Karlsruhe, KfK 4422, CNEA NT-36/87, 1988.
- [42] V. Vrtilkova, M. Valach, L. Molin, "Oxidizing and hydriding properties of Zr-1Nb cladding material in comparison with Zircalloys", Technical Committee Meeting on Influence of Water Chemistry on Fuel Cladding Behaviour, 4-8 October 1993, Prague.
- [43] L. Sepold, M. Grosse, M. Steinbrück, J. Stuckert, "Severe fuel damage experiments with advanced cladding materials to be performed in the QUENCH facility (QUENCH-ACM)", Proceedings of the 16th International Conference on Nuclear Engineering, ICONE-16, May 11-15, 2008, Orlando, Florida, USA, paper ICONE16-48054.
- [44] P. D. Parsons, E. D. Hindle and C. A. Mann, "The Deformation, Oxidation and Embrittlement of PWR Fuel Cladding in a Loss-of-Coolant Accident", OECD/NEACSNI report 129, December 1986.
- [45] T. J. Haste, B. Adroguer, U. Brockmeier, P. Hofmann, K. Müller and M. Pezzilli, "In-Vessel Core Degradation in LWR Severe Accidents, State of the Art Report Update January 1991 - June 1995", AEA/CS R1025/W, EUR 16695 EN, January 1996.
- [46] A.V. Berdyshev, A.V. Boldyrev, A.V. Palagin, V.E. Shestak, M.S. Veshchunov, "Svecha/Quench Code for The Modeling of Reflooding Phenomena in Severe Accidents Conditions", Proceedings of the Ninth International Topical Meeting on Nuclear Reactor Thermal Hydraulics (NURETH-9), paper Log_19 (CD-ROM edition), San Francisco, California, USA 1999.
- [47] Cs. Györi, Z. Hózer, K. Lassmann, A. Schubert, J. van de Laar, M. Cvan, B. Hatala: Extension of TRANSURANUS Code applicability with Niobium Containing Cladding Models (EXTRA), Proceedings of FISA-2003, EUR 21026, pp. 584-589.